

pubs.acs.org/JACS Article

Understanding Reaction Networks through Controlled Approach to Equilibrium Experiments Using Transient Methods

Yixiao Wang, Jin Qian, Zongtang Fang, M. Ross Kunz, Gregory Yablonsky, Alessandro Fortunelli, William A. Goddard III,* and Rebecca R. Fushimi*



Cite This: J. Am. Chem. Soc. 2021, 143, 10998-11006



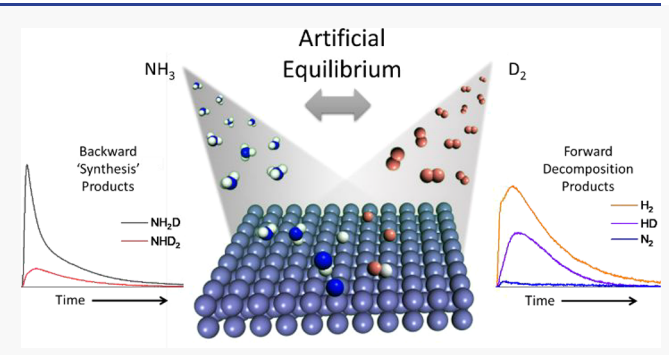
ACCESS

Metrics & More

Article Recommendations

s Supporting Information

ABSTRACT: We report a combined experimental/theoretical approach to studying heterogeneous gas/solid catalytic processes using low-pressure pulse response experiments achieving a controlled approach to equilibrium that combined with quantum mechanics (QM)-based computational analysis provides information needed to reconstruct the role of the different surface reaction steps. We demonstrate this approach using model catalysts for ammonia synthesis/decomposition. Polycrystalline iron and cobalt are studied via low-pressure TAP (temporal analysis of products) pulse response, with the results interpreted through reaction free energies calculated using QM on Fe-BCC(110), Fe-BCC(111), and Co-FCC(111) facets. In TAP experiments, simultaneous



pulsing of ammonia and deuterium creates a condition where the participation of reactants and products can be distinguished in both forward and reverse reaction steps. This establishes a balance between competitive reactions for D* surface species that is used to observe the influence of steps leading to nitrogen formation as the nitrogen product remains far from equilibrium. The approach to equilibrium is further controlled by introducing delay timing between NH_3 and D_2 which allows time for surface reactions to evolve before being driven in the reverse direction from the gas phase. The resulting isotopic product distributions for NH_2D_1 , NHD_2 , and HD at different temperatures and delay times and NH_3/D_2 pulsing order reveal the role of the N_2 formation barrier in controlling the surface concentration of NH_x^* species, as well as providing information on the surface lifetimes of key reaction intermediates. Conclusions derived for monometallic materials are used to interpret experimental results on a more complex and active CoFe bimetallic catalyst.

■ INTRODUCTION

The ammonia synthesis process supports a prosperous society by providing the primary source or nitrate based fertilizer vital for abundant food production. Moreover, ammonia can be used as a dense energy carrier where its decomposition provides the fuel hydrogen-based fuel cells. A considerable body of knowledge has been accumulated on catalytic ammonia synthesis and decomposition. This shows that the factors responsible for a good synthesis catalyst generally do not make a good decomposition catalyst generally do not make a good decomposition catalyst two processes take place with vastly different gas (and surface) compositions.

The catalyst manipulates gas and surface concentrations through a complex network of fast and slow reactions proceeding both sequentially and in parallel. At steady-state, only the slowest step is manifest limiting resolution of network details. Observation of the catalytic system under non-equilibrium conditions enables the complexity of these interworking parts to be disentangled. While such experiments may be far from the application environment, they are useful for discriminating the underlying behavior of a catalyst to

understand why one composition might perform better than another at steady-state, a necessary step in catalyst rational design. $^{9-12}$

The low-pressure TAP (temporal analysis of products) pulse response experiment sets forth a cascade of surface reactions from one direction of pulsed species in the gas phase. ^{13–15} With a singular pulse, the design of the experiment may render negligible the influence of backward reactions from the gas phase. At present, this TAP system enables only gas phase measurements, whence surface accumulation is determined indirectly, without direct observation of adsorbate configurations. To better resolve how surface reactions play out, we demonstrate in this work how to use controlled pulse timing of gas-phase species using both reactants and products of the

Received: April 1, 2021 Published: July 19, 2021





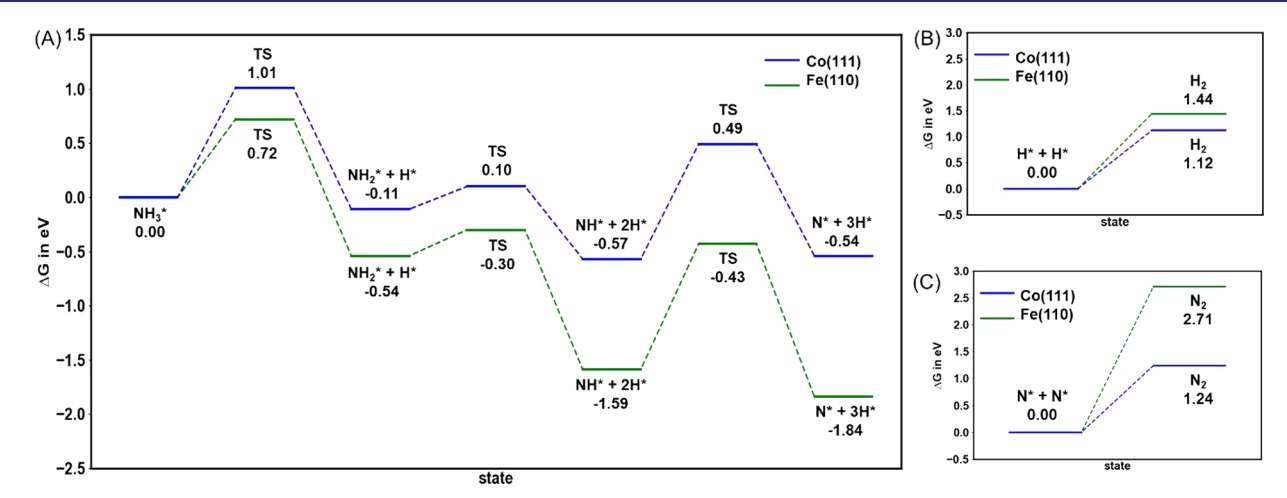


Figure 1. Free energy landscape for most abundant Fe(110) and Co(111) surfaces under experimental condition: T = 823 K, (A) NH₃ decomposition, (B) H* adsorption, and (C) N* adsorption; blue color represents Co, and green color represents Fe.

Table 1. Free Energy Barrier (ΔG with the Unit of eV) and Kinetic Rate Constant (k with the unit of s⁻¹) for Each Fundamental Step on Fe(110) and Co(111) Surfaces under the Experimental Conditions: T = 823 K, $P_{\rm NH_3} = 25$ pascal = 2.5 × 10^{-4} atm, $P_{\rm N_2} = 1.3 \times 10^{-10}$ atm, $P_{\rm H_2} = 1.3 \times 10^{-10}$ atm

			Fe(110) forward		Fe(110) back		Co(lll) forward		Co(lll) back	
	Reaction	ΔG^{\ddagger}	k	ΔG^{\ddagger}	k	ΔG^{\ddagger}	k	ΔG^{\ddagger}	k	
$k_{ m NH_3}$	$NH_3 + * \leftrightarrow NH_3*$	0.59	4.18×10^{09}	0.83	1.38×10^{08}	0.59	4.18×10^{09}	0.85	1.01×10^{08}	
k_1	$NH_3^* + * \leftrightarrow NH_2^* + H^*$	0.72	6.68×10^{08}	1.26	3.50×10^{05}	1.01	1.12×10^{07}	1.12	2.46×10^{06}	
k_2	$NH_2 + H^* + ^* \leftrightarrow NH^* + 2H^*$	0.24	5.81×10^{11}	1.30	1.95×10^{05}	0.21	8.87×10^{11}	0.67	1.38×10^{09}	
k_3	$NH^* + 2H^* + * \leftrightarrow N^* + 3H^*$	1.16	1.35×10^{06}	1.41	3.97×10^{04}	1.06	5.53×10^{06}	1.03	8.29×10^{06}	
$k_{ m N}$	$N^* + N^* \leftrightarrow N_2 + 2^*$	2.71	4.15×10^{-04}	2.11	2.17×10^{00}	1.24	4.42×10^{05}	2.11	2.17×10^{00}	
$k_{ m H}$	$H^* + H^* \leftrightarrow H_2 + 2^*$	1.44	2.74×10^{04}	2.11	2.17×10^{00}	1.12	2.51×10^{06}	2.11	2.17×10^{00}	

catalytic reaction of interest, in combination with isotopic labeling, to observe the intersection of forward and reverse surface reactions. Specifically, in our protocol we search for a unique condition in which a balance is realized between competitive reactions for a single intermediate.

We present a series of pulse response experiments using ammonia and deuterium. Polycrystalline iron and cobalt provide catalytic materials simple enough to support the interpretation of experimental results via first-principles modeling using QM. Ammonia and deuterium are pulsed simultaneously at different temperatures and with different pump/probe delay sequencing. Previously, the pump/probe TAP experiment was primarily used to examine reaction pathways between two reactants, generally hydrocarbon and oxidant. 16 In the current work, simultaneous pulsing of a reactant and a product creates an equilibrium condition between ammonia and deuterium while gas phase nitrogen remains far from equilibrium. The system approach to equilibrium is controlled by separating the pulse timing of ammonia and deuterium using a short pump/probe delay. This controlled approach allows a fixed time for surface reactions to evolve before reverse reactions are driven from the gas phase. Through the evolution of isotopically labeled products (NH₂D, NHD2, and HD), we use this method to resolve the lifetime of different surface intermediates that can be interpreted using QM predicted reaction barriers for both forward and reverse reactions. Finally, we use theoretical/experimental results for monometallic materials to understand experimental observations of the more complex bimetallic iron/cobalt catalyst and propose a rationalization for its improved activity in ammonia

decomposition, as demonstrated for other bimetallic systems. 17,18

■ RESULTS AND DISCUSSION

More details regarding the computational and experimental methods can be found in the Supporting Information.

Computational Results. The free energy landscape for ammonia decomposition to surface NH,*and H* species is presented in Figure 1A at 823 K for the Co-FCC(111) and Fe-BCC(110) surfaces which are most abundant at this temperature on bare particles. Since cobalt transitions from HCP to FCC structure near 700 K, we compare our experimental and computational results at 823 K to avoid structural ambiguity. In Figure 1A, we adopted the transition state barriers by Duan et al., 19 but we carried out separate calculations for the intermediate-state Gibbs free energy. Moreover, in the discussion we also use results on the Fe-BCC(111) surface from ref 20. We estimated adsorption free energies based on entropy corrections at 823 K and 2.5×10^{-4} atm for NH₃ and 1.3×10^{-10} atm for H₂ and N₂, conditions that are relevant to our experimental ammonia pulse response studies (for separate hydrogen pulse response studies H2 pressure of 2.5×10^{-4} atm is used). The barriers for product adsorption/desorption steps are compared with NH3 dehydrogenation steps in Table 1. Kinetic rate constants for elementary steps are obtained using the Eyring equation, i.e. assuming the Arrhenius relation between the free energy barrier, ΔG^{\ddagger} , and the rate constant, k:

$$k = \frac{k_{\rm B}T}{h} \exp\left(-\frac{\Delta G^{\ddagger}}{k_{\rm B}T}\right)$$

where $k_{\rm B}$ and h are the Boltzmann and Planck constants, respectively. Both the rate constants and free energy barriers are summarized in Table 1.

Figure 1A indicates that, at equilibrium, the dominant surface species on Fe-BCC(110) will be N* whereas on Co-FCC(111) NH* is slightly more stable than N* under the given conditions. Figure 1 shows that ammonia decomposition is more favorable thermodynamically on iron compared to cobalt. For both materials the second step of dehydrogenation $\mathrm{NH_2}^*$ to NH^* has the smallest barrier. Overall, the surface reaction barriers for iron are larger, which should result in a greater skew in the distribution of surface species.

The surface NH_x* species are depleted via competitive pathways: either forward toward the release of N₂ and H₂ or in the reverse direction toward the release of NH3. We find that the parallel steps of hydrogen (Figure 1B) and nitrogen (Figure 1C) desorption are more facile on cobalt, where we expect the coverage of both H* and N* to be lower than on iron. In contrast, the stability of N* on iron is expected to impede reaction. The barrier for nitrogen evolution on Fe-BCC(110), 2.71 eV, is higher than the experimental value ~2.17 eV on polycrystalline Fe wire at a constant NH₃, pressure of 5×10^{-6} Torr, by Ertl and Huber,²¹ but is consistent with the barrier of 2.08 eV predicted on Fe- $BCC(111).^{20}\ Note that \ N^*$ and H^* surface coverage will impact the stability of different NHx* adsorbates. In this respect, calculations on Fe-BCC(110) were conducted at low coverage as this facet is taken as a model of the Fe catalyst at low coverage of NH_x* species, but we will also use results from our prior work on Fe-BCC(111) as a model of high coverage.2

Reaction coordinate plots as in Figure 1 are useful for conveying the sequence of a process, but the impact of multiple parallel processes such as the release of N2 and H2 is better understood through microkinetic simulations. To derive a more quantitative understanding from theory, we solved a mean-field model numerically using the steps and rate constants listed in Table 1. All reaction orders were assumed to be one, and the pressure of reactants and products at time t = 0 was set to $P_{\rm NH_3}$ = 25 Pa = 2.5 × 10⁻⁴ atm, $P_{\rm N_2}$ = 1.3* 10⁻¹⁰ atm, $P_{\rm H_2} = 1.3 \times 10^{-10}$ atm at 550 °C to mimic experimental conditions of a single ammonia pulse described in the next section. These results are presented in Table S1. While the simulations include adsorption steps for the H₂ and N₂ products, these rate constants were estimated based solely on the entropy change: the relatively high values of the barriers, combined with the low concentration of these species, will emulate the nonequilibrium condition of the single pulse.

The microkinetic simulations show that N* is the most abundant surface species for iron (Table S1), as expected, while the sluggish release of H_2 results in a 10× higher H* surface concentration for Fe than Co. On cobalt, N* and H* are the most abundant and present in similar amounts. For both iron and cobalt, the low barrier for step k_2^+ results in a negligible NH₂* surface concentration. On cobalt, the free energies of NH* and N* are nearly the same, but the predicted concentration of NH* is about 3 orders of magnitude lower than N* because of the low barrier for H_2 evolution. The H_2/N_2 product ratio for cobalt is 3, in agreement with

experimental results reported under nonsteady-state conditions.²² The unfavorable barrier for nitrogen evolution on iron, 2.71 eV results in a negligible gas concentration of the N₂ product which agrees with experimental results from ammonia pulsing over Fe catalysts. 22 The sluggish release of N₂ from the iron surface is manifest experimentally by surface coverage effects and site blocking that change the probability of the forward decomposition reaction. Since we have previously shown that N* adatom accumulation also changes the relative energetics of Fe-BCC facets, 23 so that Fe-BCC(111) or Fe-BCC(100) become more stable facets than Fe-BCC(110) at high N coverage (reshaping), we model high coverage conditions using our previous work on ammonia synthesis on the Fe-BCC(111) surface.²⁰ In this prior work, the calculations were aimed at ammonia synthesis conditions in which decomposition of N2 led to N adatoms that add H atoms sequentially to make ammonia molecules. From the results of ref 20, we derive that N* is still favored on the Fe-BCC(111) surface, but at high coverage of N*, the NH₂* species becomes competitive so that the resting state of a $(2 \times$ 2) unit cell under no-reaction conditions becomes 3N·NH2 on a 2×2 surface cell (i.e., with three N* adatoms and one NH₂* species adsorbed on bridge sites). ²⁰ Moreover, under a wide set of reaction conditions the resting state configuration is 2N· NH₂·H (i.e., with two N* adatoms, one NH₂*, and one H* species adsorbed on bridge sites).

In our current experimental work, surface coverages are expected to be lower than the full coverage achieved under ammonia synthesis conditions, since we start by decomposing ammonia to form $1/2\ N_2$ (indeed, it is known that ammonia synthesis and decomposition occur at very different concentrations of ammonia). The computational results here discussed are used to interpret nonequilibrium experiments by assuming that the Fe-BCC(110) and Fe-BCC(111) facets represent idealized (perfect-facet) models of surface concentrations at low coverage and high coverage, respectively: they thus "bracket" the observed trends in the experimental, more complex situation, making them useful for rationalizing the experiments.

Comparison of computational and experimental results on monometallic materials are used to rationalize experimental trends observed for a bimetallic catalyst in the next section. Atomistic modeling of the bimetallic material is more challenging since numerous configurations and active sites may be present. But we can provide a qualitative interpretation based on the investigations on Co-doped Fe-based catalysts reported previously [corresponding to 25% surface doping of Fe-BCC(111)]²⁴ and Fe-BCC(211)R²⁵ surfaces.

Experimental Results. Separate experiments pulsing H_2 , D_2 , N_2 , and NH_3 were first performed to understand the interaction of each gas with the catalysts and to validate the modeling results. For all catalysts, we found negligible interaction of the N_2 pulse at reaction temperatures and N_2 pulses were not further utilized. Activation energies for H_2 adsorption and desorption were determined from pulse response data using the method of moments described by Shekhtman et al. (Figure S1A and S1B). The relative activation energies for iron and cobalt were in agreement with calculated desorption barriers for hydrogen (Figure S2A). Copulsing experiments of a H_2/D_2 mixture showed a prominent HD pulse response, which clearly indicates that H_2 adsorption is dissociative and reversible over these catalysts (Figure S3). In pulsing ammonia, we clearly observed the

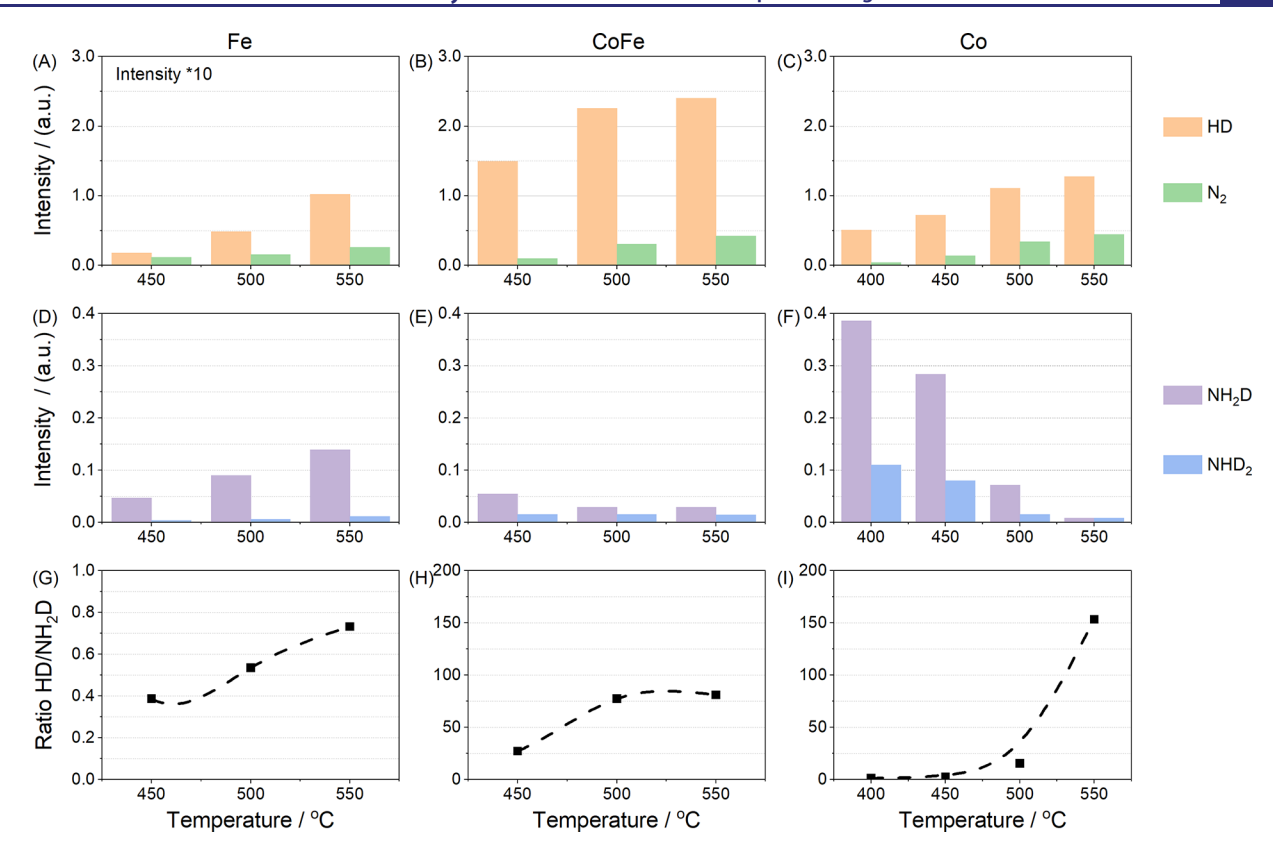


Figure 2. (A-C) HD and N_2 , (D-F) NH_2D and NHD_2 , and (G-I) relative product yield of HD and NH_2D detected during copulsing of NH_3 and D_2 over iron (A, D, and G), CoFe (B, E, and H), and Co (C, F, and I) at different temperatures.

effects of reversible adsorption in the pulse response shape of the reactant on Fe (Figure S4). The apparent activation energy for ammonia conversion was calculated from pulse response data collected at different temperatures (Figure S1C). Ammonia activation energies were higher on iron compared to cobalt containing materials, which is attributed to a higher stability of the NH* and N* species on the Fe surface that block active sites and limit conversion. The hydrogen desorption barrier was similar for Co and CoFe while the activation energy for ammonia conversion on CoFe was intermediate of each monometallic. The apparent ammonia decomposition activation energies for iron and cobalt are in agreement with the reaction barrier calculated for N2 formation (Figure S2B), which was the highest reaction barrier observed during the NH3 decomposition process (Figure 1).

Copulsed Ammonia/ D_2 Isotopic Exchange Experiments: Identifying Surface Species and Competing Processes. To create an equilibrium condition where forward and reverse steps can be distinguished, a series of experiments were conducted using copulsing of NH_3 and D_2 . First, transport-only copulsed simulations were used to verify the overlap of D_2 and NH_3 gases in the catalyst zone since D_2 will have a much higher diffusion constant (Figure S5). In copulsed experiments, we observed clear responses for isotopic products NH_2D , NHD_2 , and HD (Figure S6) while ND_3 was not observed. This confirms that both NH_3 and D_2 adsorb dissociatively.

At every temperature, the yield of H₂, HD, and N₂ was significantly lower on iron compared to CoFe and cobalt. Figure 2 displays the ammonia decomposition forward products (HD and N₂, Figure 2A–C) and reverse "products" (NH₂D and NHD₂, Figure 2 D–F) that were observed on all catalysts. The forward products show an increase in yield with

temperature for all materials (H_2 is not reported). The NH_2D and NHD_2 products result from reverse reaction steps and are shown in Figure 2D–F for each catalyst. The reverse products represent the sum of dehydrogenation followed by hydrogenation and NH_3 desorption processes. For all materials, NH_2D (single exchange) is formed in greater amounts than NHD_2 (double exchange).

With both forward and reverse isotopic products observed, it is clear that a "decision point" exists for a surface D* species to either continue forward to release HD or to combine with an NH $_x$ surface species leading to the desorption of NH $_2$ D. From the reaction barriers in Table 1, we note that the barriers for H association and evolution of H $_2$ are very similar to the highest barrier for hydrogenation in the reverse direction. More specifically, on iron the forward barrier for H $_2$ formation is 1.44 eV while the first hydrogenation step, k_3^- , N* + H* \rightarrow NH* + *, is highest in the reverse direction, 1.41 eV. On cobalt, the forward and reverse barriers are identical, 1.12 eV, with the highest hydrogenation barrier occurring at the last step before NH $_3$ release, k_1^- , NH $_2^+$ + H* \rightarrow NH $_3^+$ + *. From this perspective, if the surface concentrations are the same, then the forward and reverse reactions are similarly probable.

The experimental trends of the NH_2D and HD products for iron are shown in Figure 2A and D. We observe that product intensities have similar temperature trends and are similar in magnitude, with NH_2D being slightly favored. Similarly, for cobalt, Figure 2C and F show that the forward and reverse products also have a similar magnitude at low temperatures (400 °C) with HD being slightly favored. However, as temperature increases, the HD formation increases while the reverse reaction NH_2D product is strongly diminished; hence, the HD/NH_2D ratio dramatically increases over Fe (Figure

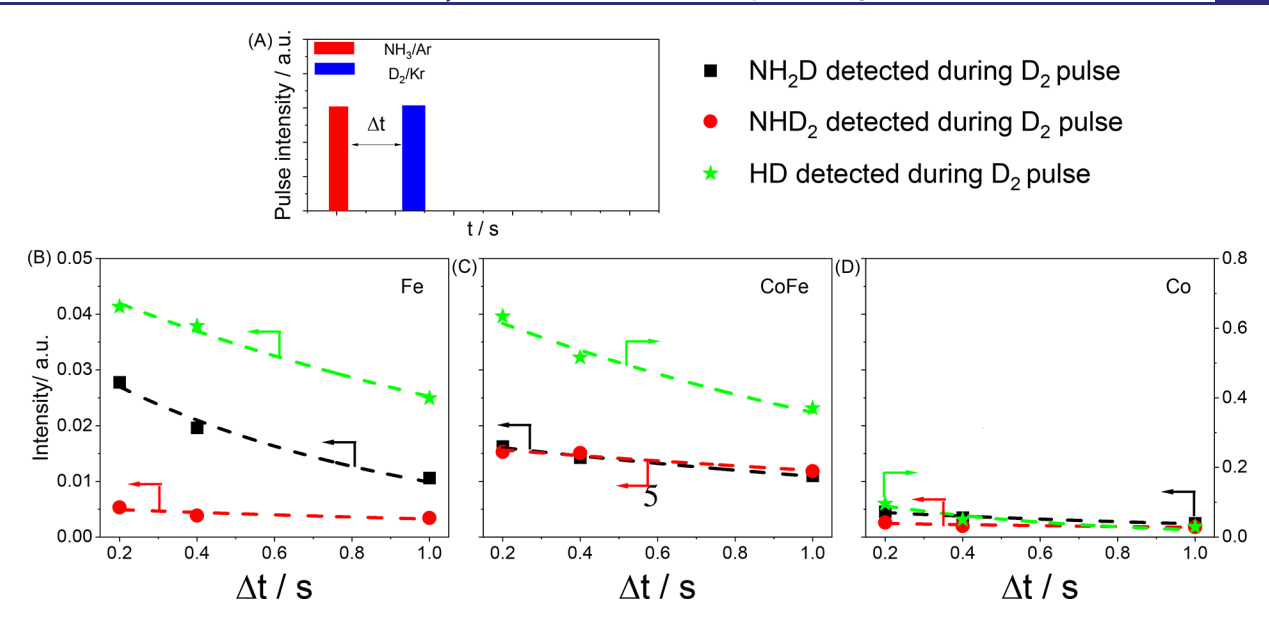


Figure 3. (A) Definition of pump-probe experiments with two injection valves at 550 °C. Pump molecules: NH₃. Probe molecules: D₂. The pulse size normalized intensity of NH₂D, NHD₂, and HD intensity versus the pump probe delay time (Δt) over (B) Fe, (C) CoFe, and (D) Co.

2G) and Co (Figure 2I). Generally, the formation of HD at the expense of NH₂D would indicate competition for a common intermediate, i.e. D*. Recalling however that the forward and reverse reaction barriers for HD and NH2D formation are identical on cobalt, we conclude that surface concentration must also factor into the rate of transformation/yield and that the lower formation of NH₂D at high temperature is associated with a lower surface concentration of NH_x* species on cobalt due to the low barrier for N2 formation, 1.24 eV. In the case of iron, the NHx* concentration will be much higher due to a considerable N2 formation barrier, 2.71 eV (or 2.08 eV depending on the facet) and to the favorable energetics of NH₂* species on Fe-BCC(111). Thus, on cobalt, the observed temperature trends for NH₂D formation are understood to result from the temperature dependence of the N2 formation step, whereas the similar temperature trends for both products on iron indicates that control lies in either the adsorption or decomposition steps. By comparing the behavior of each material under these unique conditions, the relative reaction barriers for the entire decomposition process are better understood.

We can exploit these observations on iron and cobalt to rationalize the experimental results for CoFe where the uncertainties in surface composition can make quantitative calculations more difficult. Figure 2B and E show that, strikingly, CoFe has the highest HD formation compared to either monometallic materials (Figure 2A and C) and the HD/ NH₂D ratio is also significantly higher at lower temperatures (Figure 2H). This is supported by the high conversion observed for NH₃ and the low barrier measured for H₂ desorption. However, the amount of N2 formed is similar to that observed on cobalt. The temperature dependence of NH₂D production is weak indicating that the surface coverage of N may not be as strongly affected by the N2 formation barrier as we observed for iron (where the barrier is high) and cobalt (where the barrier is low). The value of the N₂ formation barrier for CoFe can thus be assumed to be intermediate of those observed for each monometallic. This agrees with the experimentally measured activation energy for NH₃ conversion where CoFe is intermediate between iron and

cobalt, Figure S2B. Thus, the major impact of the bimetallic formulation results from changes in the barriers associated with hydrogen rather than nitrogen.

Isotopic Pump/Probe Experiments: Distinguishing the Lifetime of Surface Species. To investigate more closely the relative reaction barriers, a series of pump/probe experiments were conducted to measure the surface residence time of H^* and NH_x^* species. The experimental format consists of separating the introduction of two reactants from separate valves by a finite time delay, Δt . The primary (pump) pulse establishes a cascade of surface reactions which are interrogated following different time delays by the secondary (probe pulse). In this manner, the probe pulse samples the kinetic state at different times during the evolution of the surface composition in response to the primary pulse.

In the first set of experiments, NH₃ was pulsed followed by D₂ using a time delay of 0.2, 0.4, or 1.0 s (Figure 3A). Compared to the copulsed experiment, this scheme changes the approach to equilibrium by allowing a controlled time period for surface reactions to take place before reverse reactions are then driven from the gas phase by the probe pulse. The relative intensities for NH₂D, NHD₂, and HD isotopic products are presented in Figure 3B-D. The primary ammonia pulse sets forth the decomposition reaction and formation of NH₂*, NH*, H*, and N* species on the surface which the D₂ probe pulse can then interact with. Changing the time delay for introduction of D2 changes the isotopic product distribution according to the "snapshot" of NHx* surface species that have evolved from the initial the NH₃ pulse. As shown in Figure 3B-D, at 550 °C, the intensity of all products decreases with delay time on all three materials. We consistently observe a large change between simultaneous pulsing (Figure 2D-F) and the pump/probe delay time 0.2 s (Figure 3B-D) that exceeds the decay rate observed with increasing delay time. This can be rationalized by a higher number of turnovers for a fast reaction when both gases in the catalyst zone significantly overlap.

On the cobalt samples, NH_2D and NHD_2 reverse product formation exceeded the surface lifetime of NH_x^* species on this surface (Figure 3D). This is confirmed by insignificant

detection at delay times greater than 0.2 s. In contrast, the iron sample showed a gradual decrease in NH₂D with formation still detected at 1.0 s (Figure 3B). While NHD₂ formation shows a decreasing trend and is not detected after 0.4 s. A similar decay in HD formation with H* from NH₃ dehydrogenation persisting as long as 1.0 s when it combines with D* molecules from the D₂ pulse. The amount of HD formation on iron is significantly lower compared to the large production on CoFe (Figure 3B and C) but also lower than on and cobalt (Figure 3D). On iron, when NH₃ and D₂ are pulsed simultaneously, NH₂D production is slightly more abundant than that of HD (Figure 3A). However, with introduction of a time delay for the D₂ pulse, HD becomes the more abundant product (Figure 3A). This inversion may be attributed by a short lifetime of NH₂* species that are detected by deuteration in simultaneous pulsing. Additionally, on the longer time-scale of the pump/probe experiment, NH2* is dehydrogenated and proceeds to NH* before the introduction of the D₂ pulse. HD formation is then more abundant, but the NH* species may still be hydrogenated with both H* and D* to release NH2D in lesser amounts (see the discussion below).

To discuss the lifetime of different surface species, the following simplified reversible scheme for dehydrogenation isotopic exchange and hydrogenation can be considered (all steps are surface reactions; some H species are mere spectators, and active sites, *, have been removed for clarity):

Scheme I.
$$NH_3 \stackrel{k_1}{\rightarrow} NH_2 + H \stackrel{k_2}{\rightarrow} NH + 2H \stackrel{k_3}{\rightarrow} N + 3H$$
 Forward Scheme II. $NH_2D \stackrel{k_{-1}}{\leftarrow} NH_2 + D$ $\stackrel{\mathcal{E} \times 2}{\leftarrow} D$ $\stackrel{\mathcal{E} \times 2}{\leftarrow} D$ Reverse Scheme IV. $NH_2D \stackrel{k_{-1}}{\leftarrow} NDH + H \stackrel{k_{-2}}{\leftarrow} ND + 2H \stackrel{k_{-3}}{\leftarrow} N + 2H + D$

Here, ammonia is sequentially dehydrogenated in steps k_1 , k_2 , and k_3 forming NH₂*, NH*, and N* surface species (Scheme I). Isotope exchange can take place at any of these three steps and will be detected as NH₂D following the reverse hydrogenation steps, k_{-3} , k_{-2} , and k_{-1} . We simplify the argument by first considering only a singular H–D exchange and seek to determine if one can experimentally distinguish if D was added to the N*, NH*, or NH₂* species.

First, we find that NH₂D formation via Scheme IV is not observed; i.e., the N* species is not deuterated in k_{-3} . In separate experiments where samples were pretreated with ¹⁵ND₃, to generate abundant surface ¹⁵N*, subsequent pulsing of D₂ did not generate ¹⁵ND₃. Furthermore, temperatureprogrammed desorption experiments of the iron sample pretreated with 10,000 pulses of ¹⁵ND₃ at 550 °C showed a maximum ¹⁵N₂ formation peak at 750 °C. This indicates that the iron sample does retain 15N* species that are not easily hydrogenated. For cobalt, it has been described that accumulated N* can form Co₄N which is decomposed at 620 °C.²⁷ The computational result, Figure 1, supports this conclusion as multiple stepwise hydrogenation from N* (Scheme IV) is unlikely to form ND3 since N is a significantly stable structure (-1.84 eV) in the energy landscape of Fe-BCC(110), and also of Fe-BCC(111). On Co-FCC(111), the NH* and N* species are nearly degenerate whereas N* was previously reported as significantly more stable than NH* on Fe-BCC(111).²⁰ To be more specific, in order to make ammonia species from N*, a global energy barrier as high as 2.56 eV must be overcome on Fe-BCC(110).

Thus, NH₂D is predominantly formed from addition of deuterium to either NH₂* or NH* in either Scheme II or III as listed above. As shown in Table 1, the barrier for NH₂* to decompose into NH* and H* is as low as 0.24 eV on Fe-BCC(110) and 0.21 eV on Co-FCC(111). Therefore, NH₂* has a very short lifetime on these surfaces. Prior work on Fe-BCC(111) however shows that NH₂* is a significantly abundant species at high coverage²⁰ and indeed the NH₂D product may uniquely prevail over HD on the iron catalyst. By pulsing D₂ and NH₃ simultaneously on iron, the added D is able to detect the NH_2^* species via k_{-1} in Scheme II before it is further dehydrogenated via k_2 ; in this case NH₂D is the most abundant product. However, by adding a delay time in the pump/probe spacing, dehydrogenation proceeds to NH* which can still be detected via backward reaction in Scheme III after time durations up to 1.0 s on iron. NH₂D product formation is diminished when a delay time is imposed due to three competing routes: hydrogenation with H* via Schemes II and III and dehydrogenation via k_3 to N*. This extended surface lifetime of NH* observed in experiments agrees with the thermodynamic well found in Figure 1 for iron. Moreover, the microkinetic modeling result estimates that the NH* concentration is $10^7 - 10^6$ orders of magnitude higher than the NH₂* concentration (Table S1) on Fe-BCC(110) and Co-FCC(111); respectively. To summarize, the N* species does not participate and the lifetime of the NH₂* species is beyond the time resolution of the experiments presented here. For the iron sample, a half-life of 0.6 s can be attributed to the NH* species from the NH₂D pump/probe decay curve in Figure 3B. The CoFe or cobalt samples require data collected at delay time <0.2 s or lower temperatures for reliable NH* half-life prediction (Figure 3C and D).

The same approach can be used to understand NHD_2 formation where double H-D exchange takes place. In fact, the formation of NHD_2 further emphasizes the role of the NH^* species on iron, where direct addition of two atoms from the same D_2 molecule provides the simplest route. We can expect the decay of ND_2H in Figure 3 to have the same time constant as NH_2D and a lower abundance based on the concentration of D^* species. However, the present data set is too sparse to reach a reliable conclusion.

From the HD decay curves, the half-life of H* originating from NH₃ is found in Table 2 for each material. HD decay is faster in Figure 3 for cobalt compared to iron, which agrees

Table 2. Half-life (s) Associated with Surface Species Originating from Different Probe Molecules on Catalysts at 550 $^{\circ}$ C^a

	Catalysts								
	Fe		CoF	e	Со				
Surface species	Half-life (s)	R^2	Half-life (s)	R^2	Half-life (s)	R^2			
NH* from NH ₃	0.6	0.98	<0.2	-	<0.2	-			
H* from NH ₃	1.1	0.99	2.8	0.89	0.5	0.89			
D^* from D_2	3.6	0.90	1.9	0.88	Insufficient data	-			

"Includes correlation coefficient (R^2) of data and exponential fit. NH* is calculated from the NH₂D decay in Figure 3, H* is calculated from the HD decay in Figure 3, and D* is calculated from the NH₂D decay on iron and HD decay on CoFe in Figure S7.

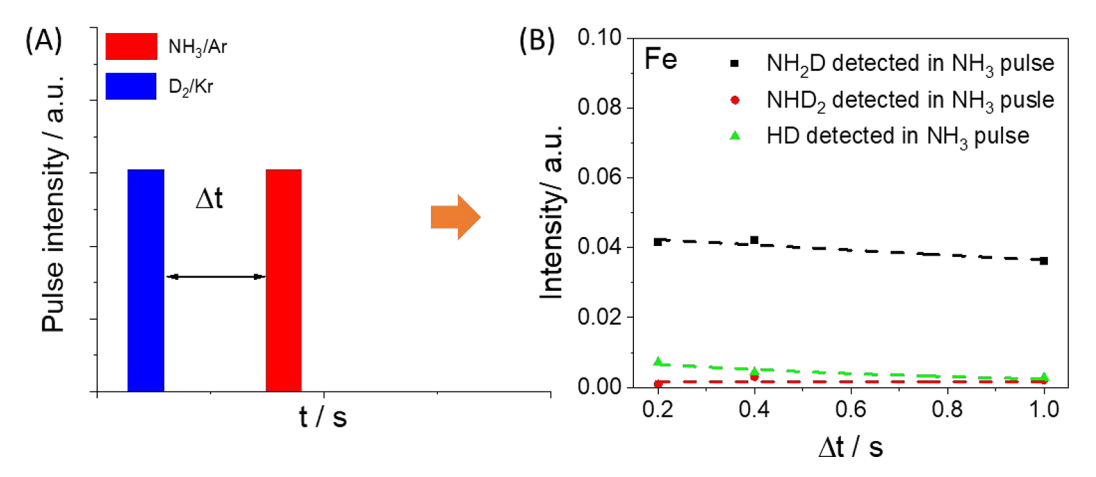


Figure 4. (A) Definition of pump-probe experiments with two injection valve, pump molecules: D_2 , probe molecules: NH_3 . (B) Intensity of NH_2D , NHD_2 , and HD intensity versus the pump probe delayed time (Δt) over Fe.

with the lower barrier for H_2 evolution on cobalt in Table 1. Strikingly, however, the bimetallic material demonstrates significantly higher HD yields (see also Figure 2B) and a longer half-life than either monometallic component.

In a second set of experiments, the pump/probe format (order) was reversed with a D_2 pulse followed by a NH_3 pulse (Figure 4A). This is used to determine the surface lifetime of species originating from D_2 . Figure 4B shows the relative product intensities as a function of the pump/probe delay spacing in the reverse format. Product intensity data in this experiment were reported on the NH_3 probe pulse. From the results on singular D_2 pulses, we know that the concentration of D^* species is controlled by reversible D_2 adsorption (Figures S1 and S2). D_2 is easily dissociated, forming D^* , and by changing the delay time (Δt), the surface lifetime of D can be observed as the isotopic products detected with the probe pulse diminish. On all samples, deuterated products can be detected at extended intervals: 1.0, 2.5, and 0.4 s for iron (Figure 4B), CoFe, and cobalt (Figure S7), respectively.

On the iron sample, in Figure 4B, the intensity of NH₂D was higher than HD which is representative of the short-lived NH₂* species that quickly reacts with available D* when ammonia is pulsed. Both the NH₂D and HD formation on iron drops sharply between the first two points. With increasing delay times, NH2D formation on iron shows a slow decline which indicates the persistence of the D* species from the D₂ pulse. From the decay of NH₂D, the half-life of D* on iron can be estimated at 3.6 s. This D* species in the primary pulse will be available to react with either ammonia dissociation product, NH₂* or H*. Using the argument for near equitable barriers for forward and reverse, i.e. 1.44 eV for $k_{\rm H}^+$ and 1.41 for k_3^- , the direction of the observed reaction is dependent on the concentration of NH_x species; also recall previous arguments surrounding the temperature-dependent trends in Figure 2. The preferred product follows the molecule in the probe pulse; that is, HD is the primary product when D₂ is pulsed to probe the NH₂* surface and NH₂D is the primary product when NH₂ is pulsed to probe the D* covered surface. This again reflects the fact that the surface lifetime of H* or (D*) is much greater than NH2*. In other words, if NHx is available on iron, D* prefers to form NH₂D as opposed to HD which agrees with the slightly lower barrier for k_3^- . However, if NH_x remains on the surface, HD will be observed since NH_x is converted to more stable N* species that are unavailable for reaction.

As indicated in Table 2, the half-life of D* from D_2 is longer than that detected for H* originating from NH₃. This distinction arises from the availability of the NH₂* species in each experiment. In the NH₃/D₂ experiment the NH₂* species is allowed time to convert to both NH* and H*. On iron, these species decrease in concentration with a half-life of 0.6 and 1.1 s, respectively. In this case, H* can be consumed through multiple pathways leading back to NH₃ and forward to HD. In the D_2/NH_3 experiment, D* is available for reaction and associates with NH₂* before this species is further dehydrogenated. As described previously, on iron, the D* species favors association with NH₂* over H*, HD formation is insignificant (Figure 4B), and only one path exists to NH₂D for the depletion of D* in the D_2/NH_3 experiment.

CONCLUSIONS

With only three gas phase species, the ammonia synthesis/ decomposition chemistry presents a relatively simple case for examining how different catalysts control reaction barriers through manipulation of nonequilibrium conditions in transient experiments. Under low pressure conditions, the TAP pulse response of ammonia can be used to drive the chemistry forward from the gas phase or backward by pulsing hydrogen (or deuterium). While the evolution of surface reactions will proceed in both directions, the relative barriers and role of different surface species were resolved here using isotopic labeling and manipulation of the approach to equilibrium between only ammonia and deuterium. Nitrogen gas was kept out of equilibrium, and the changes in the isotopic product distribution of NH₂D, NHD₂, and HD were used to resolve the relative reaction barriers for both forward and reverse directions on the catalyst surface.

This work presents a unique vantage point for studying ammonia synthesis surface reaction steps under low pressure, which would normally be thwarted by the low N_2 sticking coefficient. QM-predicted reaction barriers assisted in the interpretation of these results for simple polycrystalline iron and cobalt catalysts. Thermodynamic barriers indicated a "decision point" where the H* (or D* species used experimentally) finds nearly equal barriers in forward and reverse directions toward the gas phase, i.e., either combining with NH_x^* leading to NH_2D or combining with H* leading to HD. Experimentally, a balance of competitive reactions for a single surface intermediate (D^*) was found with the system

controlled by the reaction step associated with the N_2 product that remained far from equilibrium. By pulsing NH_3 and D_2 simultaneously at different temperatures and in controlled pump/probe delay timing, the influence of the reaction barriers that control surface species concentration were observed.

On cobalt, trends in NH₂D and HD formation result from the temperature dependence of the N₂ formation step. On iron, the high barrier for N₂ desorption keeps the surface concentration of NH_x species high and temperature trends for products are controlled by ammonia adsorption. While the NH* species was the primary reactive intermediate on iron and isothermal pump/probe delay experiments indicated a half-life of 0.6 s, the participation of the shorter-lived NH₂* species was observed during simultaneous and D₂/NH₃ delay pulsing. The half-life of D* originating from D2 and H* from NH3 were similarly observed for different catalysts. We find different values depending on the experimental format due to the presence/absence of NH₂*. Both theoretical and experimental results from the monometallic materials were used to rationalize experimental results for the more complex CoFe bimetallic catalyst. By adding cobalt to the surface of iron, experimental results conclude that the improved performance of the bimetallic can be attributed to the reduction in the hydrogen formation barrier.

While pulse response experiments under low pressure conditions have been established as a means for precise kinetic characterization, these methods are restricted to measurement from the gas phase and surface species are not directly observed. However, this work demonstrates that manipulation of the approach to equilibrium, through precise pulse timing of isotopic labels of both reactants and products (in both direct and reverse order), provides a new approach for understanding how the network of surface reaction steps unfold on complex industrial catalysts as well as for deriving quantitative data on lifetimes of surface species and kinetic constants of individual surface reactions.

ASSOCIATED CONTENT

Supporting Information

The Supporting Information is available free of charge at https://pubs.acs.org/doi/10.1021/jacs.1c03158.

Catalyst preparation and characterization methods. Computational methods. Experimental methods including TAP reactor description and pulse response methods. Microkinetic modeling results. H_2 and NH_3 Arrhenius plots. H_2/D_2 copulsing experimental results. Time-dependent rate of the ammonia conversion during one pulse response. Transport simulation for copulsed experiments. Response of forward and reverse products during NH_3 and D_2 copulsing. Half-life calculation method. D_2 and NH_3 pump/probe experimental results. Catalyst characterization results. (PDF)

AUTHOR INFORMATION

Corresponding Authors

Rebecca R. Fushimi — Biological and Chemical Science and Engineering Department, Idaho National Laboratory, Idaho Falls, Idaho 83415, United States; orcid.org/0000-0002-7570-0234; Email: Rebecca.fushimi@inl.gov

William A. Goddard III – Materials and Process Simulation Center, California Institute of Technology, Pasadena,

California 91125, United States; o orcid.org/0000-0003-0097-5716; Email: wag@caltech.edu

Authors

Yixiao Wang — Biological and Chemical Science and Engineering Department, Idaho National Laboratory, Idaho Falls, Idaho 83415, United States; orcid.org/0000-0002-1446-3634

Jin Qian – Materials and Process Simulation Center, California Institute of Technology, Pasadena, California 91125, United States; Chemical Sciences Division, Lawrence Berkeley National Laboratory, Berkeley, California 94720, United States

Zongtang Fang — Biological and Chemical Science and Engineering Department, Idaho National Laboratory, Idaho Falls, Idaho 83415, United States; orcid.org/0000-0001-6034-1083

M. Ross Kunz — Biological and Chemical Science and Engineering Department, Idaho National Laboratory, Idaho Falls, Idaho 83415, United States

Gregory Yablonsky — Department of Energy, Environmental and Chemical Engineering, Washington University in St. Louis, Saint Louis 63130, United States

Alessandro Fortunelli — Materials and Process Simulation Center, California Institute of Technology, Pasadena, California 91125, United States; CNR-ICCOM, Consiglio Nazionale delle Ricerche, Pisa 56124, Italy; ocid.org/ 0000-0001-5337-4450

Complete contact information is available at: https://pubs.acs.org/10.1021/jacs.1c03158

Notes

The authors declare no competing financial interest.

ACKNOWLEDGMENTS

This work was supported by U.S. Department of Energy (USDOE), Office of Energy Efficiency and Renewable Energy (EERE), Advanced Manufacturing Office Next Generation R&D Projects under Contract No. DE-AC07-05ID14517. The authors express gratitude to Dickson Ozokwelu for his support and dedicate this manuscript to his memory. In addition, A.F. and W.A.G. received support from NSF (CBET-1805022 and CBET-2005250).

REFERENCES

- (1) Appl, M. Ammonia. Ullmann's Encyclopedia of Industrial Chemistry; Wiley-VCH: Weinheim, Germany, 2006.
- (2) Zhang, J.; Comotti, M.; Schüth, F.; Schlögl, R.; Su, D. S. Commercial Fe-or Co-containing carbon nanotubes as catalysts for NH 3 decomposition. *Chem. Commun.* **2007**, No. 19, 1916–1918.
- (3) Chen, J. G.; Crooks, R. M.; Seefeldt, L. C.; Bren, K. L.; Bullock, R. M.; Darensbourg, M. Y.; Holland, P. L.; Hoffman, B.; Janik, M. J.; Jones, A. K. Beyond fossil fuel-driven nitrogen transformations. *Science* **2018**, *360*, *6391*.
- (4) Choudhary, T.; Sivadinarayana, C.; Goodman, D. Catalytic ammonia decomposition: COx-free hydrogen production for fuel cell applications. *Catal. Lett.* **2001**, 72 (3), 197–201.
- (5) Yin, S.; Xu, B.; Zhou, X.; Au, C. A mini-review on ammonia decomposition catalysts for on-site generation of hydrogen for fuel cell applications. *Appl. Catal., A* **2004**, *277* (1–2), 1–9.
- (6) Boisen, A.; Dahl, S.; Nørskov, J. K.; Christensen, C. H. Why the optimal ammonia synthesis catalyst is not the optimal ammonia decomposition catalyst. *J. Catal.* **2005**, 230 (2), 309–312.

- (7) Matera, S.; Schneider, W. F.; Heyden, A.; Savara, A. Progress in Accurate Chemical Kinetic Modeling, Simulations, and Parameter Estimation for Heterogeneous Catalysis. *ACS Catal.* **2019**, *9* (8), 6624–6647.
- (8) Constales, D.; Yablonsky, G. S.; D'hooge, D. R.; Thybaut, J. W.; Marin, G. B. Advanced data analysis and modelling in chemical engineering; Elsevier: 2016.
- (9) Toyao, T.; Maeno, Z.; Takakusagi, S.; Kamachi, T.; Takigawa, I.; Shimizu, K.-i. Machine Learning for Catalysis Informatics: Recent Applications and Prospects. ACS Catal. 2020, 10 (3), 2260–2297.
- (10) Mendes, P. S. F.; Siradze, S.; Pirro, L.; Thybaut, J. W. Open Data in Catalysis: From Today's Big Picture to the Future of Small Data. *ChemCatChem* **2021**, *13* (3), 836–850.
- (11) Wang, P.; Chang, F.; Gao, W.; Guo, J.; Wu, G.; He, T.; Chen, P. Breaking scaling relations to achieve low-temperature ammonia synthesis through LiH-mediated nitrogen transfer and hydrogenation. *Nat. Chem.* **2017**, *9* (1), 64–70.
- (12) Mao, C.; Li, H.; Gu, H.; Wang, J.; Zou, Y.; Qi, G.; Xu, J.; Deng, F.; Shen, W.; Li, J.; Liu, S.; Zhao, J.; Zhang, L. Beyond the Thermal Equilibrium Limit of Ammonia Synthesis with Dual Temperature Zone Catalyst Powered by Solar Light. *Chem.* **2019**, *5* (10), 2702–2717
- (13) Pérez-Ramírez, J.; Kondratenko, E. V. Evolution, achievements, and perspectives of the TAP technique. *Catal. Today* **2007**, *121* (3–4), 160–169.
- (14) Morgan, K.; Maguire, N.; Fushimi, R.; Gleaves, J.; Goguet, A.; Harold, M.; Kondratenko, E.; Menon, U.; Schuurman, Y.; Yablonsky, G. Forty years of temporal analysis of products. *Catal. Sci. Technol.* **2017**, 7 (12), 2416–2439.
- (15) Gleaves, J. T.; Yablonsky, G.; Zheng, X.; Fushimi, R.; Mills, P. L. Temporal analysis of products (TAP)—recent advances in technology for kinetic analysis of multi-component catalysts. *J. Mol. Catal. A: Chem.* **2010**, *315* (2), 108–134.
- (16) Perez-Ramirez, J.; Kondratenko, E. V. Evolution, achievements, and perspectives of the TAP technique. *Catal. Today* **2007**, *121* (3–4), 160–169.
- (17) Simonsen, S. B.; Chakraborty, D.; Chorkendorff, I.; Dahl, S. Alloyed Ni-Fe nanoparticles as catalysts for NH3 decomposition. *Appl. Catal., A* **2012**, 447–448, 22–31.
- (18) Duan, X.; Ji, J.; Yan, X.; Qian, G.; Chen, D.; Zhou, X. Understanding Co-Mo Catalyzed Ammonia Decomposition: Influence of Calcination Atmosphere and Identification of Active Phase. *ChemCatChem* **2016**, *8* (5), 938–945.
- (19) Duan, X.; Ji, J.; Qian, G.; Fan, C.; Zhu, Y.; Zhou, X.; Chen, D.; Yuan, W. Ammonia decomposition on Fe (1 1 0), Co (1 1 1) and Ni (1 1 1) surfaces: A density functional theory study. *J. Mol. Catal. A: Chem.* **2012**, 357, 81–86.
- (20) Qian, J.; An, Q.; Fortunelli, A.; Nielsen, R. J.; Goddard III, W. A. Reaction mechanism and kinetics for ammonia synthesis on the Fe (111) Surface. *J. Am. Chem. Soc.* **2018**, *140* (20), 6288–6297.
- (21) Ertl, G.; Huber, M. Mechanism and kinetics of ammonia decomposition on iron. *J. Catal.* **1980**, *61* (2), 537–539.
- (22) Wang, Y.; Kunz, M. R.; Siebers, S.; Rollins, H.; Gleaves, J.; Yablonsky, G.; Fushimi, R. Transient kinetic experiments within the high conversion domain: the case of ammonia decomposition. *Catalysts* **2019**, *9* (1), 104.
- (23) An, Q.; McDonald, M.; Fortunelli, A.; Goddard III, W. A. Controlling the Shapes of Nanoparticles by Dopant-Induced Enhancement of Chemisorption and Catalytic Activity: Application to Fe-Based Ammonia Synthesis. ACS Nano 2021, 15 (1), 1675–1684.
- (24) Qian, J.; Fortunelli, A.; Goddard III, W. A. Effect of Co doping on mechanism and kinetics of ammonia synthesis on Fe (1 1 1) surface. *J. Catal.* **2019**, *370*, *364*–*371*.
- (25) Fuller, J.; Fortunelli, A.; Goddard III, W. A.; An, Q. Discovery of Dramatically Improved Ammonia Synthesis Catalysts through Hierarchical High-Throughput Catalyst Screening of the Fe (211) Surface. *Chem. Mater.* **2020**, 32 (23), 9914–9924.

- (26) Shekhtman, S. O.; Yablonsky, G. S.; Gleaves, J. T.; Fushimi, R. State defining" experiment in chemical kinetics—primary characterization of catalyst activity in a TAP experiment. *Chem. Eng. Sci.* **2003**, 58 (21), 4843–4859.
- (27) Yao, Z.; Zhu, A.; Chen, J.; Wang, X.; Au, C.; Shi, C. Synthesis, characterization and activity of alumina-supported cobalt nitride for NO decomposition. *J. Solid State Chem.* **2007**, *180* (9), 2635–2640.